A USRP-based Channel Sounder for UAV Communications

Zhang, Guojin; Cai, Xuesong; Fan, Wei; Pedersen, Gert Frølund

Published in:
2020 14th European Conference on Antennas and Propagation (EuCAP)

DOI (link to publication from Publisher):
10.23919/EuCAP48036.2020.9135251

Publication date:
2020

Document Version
Accepted author manuscript, peer reviewed version

A USRP-Based Channel Sounder for UAV Communications

Guojin Zhang, Xuesong Cai*, Wei Fan, and Gert Frølund Pedersen
Antennas, Propagation and Millimetre-wave Systems (APMS) section
Department of Electronic Systems, Aalborg University, Aalborg, 9220, Denmark.
E-mail address:{guojin,xuc,wfa,gfp}@es.aau.dk.

***Abstract*—The unmanned-aerial-vehicle (UAV) has attracted great interests in both civil and military applications, due to its low cost, flexibility and ability to establish seamless coverage. In this paper, a Universal Software-defined Radio Peripheral (USRP) based channel sounding system for characterizing the UAV communication channel is introduced, which can be applied in both active and passive measurement campaigns. To investigate the effect of the equipment in the UAV measurement system, measurements were conducted by connecting two USRP devices directly with a cable. Furthermore, a post-processing method is proposed to calibrate the delay shift and "fake" Doppler frequency caused by the frequency deviation of the local oscillator in the system.**

***Index Terms*—unmanned-aerial-vehicle (UAV), channel sounding, delay shift, and "fake" Doppler frequency.**

I. Introduction

With their flexibility and low cost, unmanned-aerial-vehicles (UAVs), also commonly known as drones or remotely piloted aircrafts, have gained significant interests in both industry and academia [1]. UAVs are now widely used in civil and commercial applications, such as video surveillance, weather monitoring, search and rescue operations, precision farming, and transportation [2]. Among these applications, the use of UAVs for achieving high-speed wireless communications is expected to play an important role in future communication systems [3].

Extensive measurement campaigns have been conducted for characterizing the UAV communication channel, which is important for the performance evaluation and design of UAV communication systems [4]–[8]. Most of the measurement campaigns were conducted in urban, suburban and open fields with mostly clear line-of-sight (LOS) scenarios such as mountain, desert, hilly and over-sea, etc. Furthermore, the choice of channel sounding equipment is important, considering the on-board space limitations, payload weight, bandwidth requirements and multipath resolution. Time Domain P440 radios were used for ultrawideband (UWB) channel sounding in bi-static mode with the operating frequency from 3.1 GHz to 5.3 GHz [9]. In [10], an autonomous mobile network scanner by Rohde & Schwarz was chosen for recording the live LTE signals at the 800 MHz frequency band, which is capable of reporting radio measurements from up to 32 cells per recorded sample. Smartphones are also applied for the test of EDGE, HSPA+ and LTE technologies [11], [12]. The millimeter-wave (mmWave) spectra measurement campaign at 28 and 38 GHz was planned to be conducted using SAFtehnika 24-40 GHz mmWave portable spectrum analyser [13]. Moreover, Universal Software-defined Radio Peripheral (USRP) hardware is widely applied in UAV measurement campaigns, such as N-210 [4], [14], B-210 [5], X-310 [6], [7] and B-200 mini, which are benefit with their lighter weight, software-definability, and ability to test multi-carrier and MIMO system in UAV communication.

In this paper, a USRP-based channel sounding system for characterizing the UAV communication channel is introduced. This paper aims to investigate the effect of the system equipment on the measured signals. The first issue is the possible effect introduced by the system responses of the USRP devices and cable. The second issue is the frequency offset caused by the local oscillator of USRP. The rest of this paper is organized as follows. In Sect. II, the components of a USRP-based channel sounding system are introduced. Sect. III analyzes the system response by the measurements connecting two USRPs with a cable directly. Sect. IV elaborates the method for eliminating the frequency offset caused by the local oscillator. Finally, concluding remarks are given in Sect. V.

II. Measurement System

Fig. 1(a) illustrates the block diagram of the UAV measurement system, which consists of two parts, i.e., the air part and the ground part as shown in Fig. 1(b) and Fig. 1(c), respectively. The UAV measurement system can be used for both active and passive channel sounding measurements as shown in Fig. 2. Note that the term "active" here means that we transmit and receive the signals by ourselves, and "passive" means that we receive the signals already existing in the environment. The active channel sounding can be applied for the air-to-ground (A2G) and air-to-air (A2A) propagation measurement campaigns, and the passive channel sounding can be applied for collecting the down-link signals from base stations (BSs) such as in commercial 3G and 4G networks.

The air part contains an antenna, a USRP device of type N210, a computer, a commercial wireless fidelity (WiFi) router, a Global Positioning System (GPS) disciplined oscillator and a GPS antenna. The ground part includes the same components as the air part and a computer for controlling the air part. Local area network can be built by the two commercial WiFi

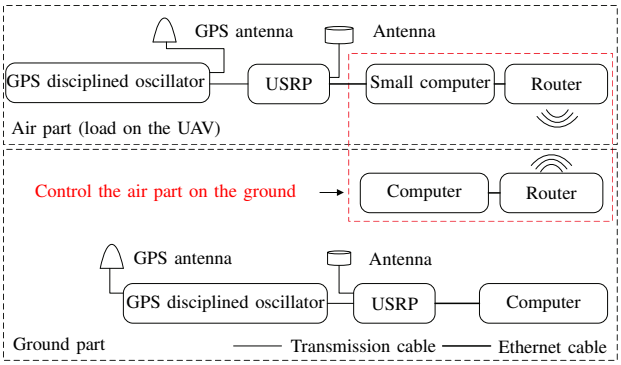

(a)

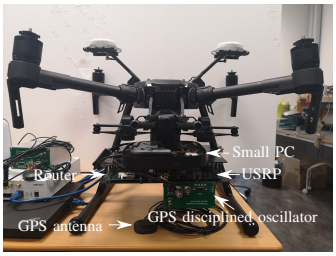

(b)

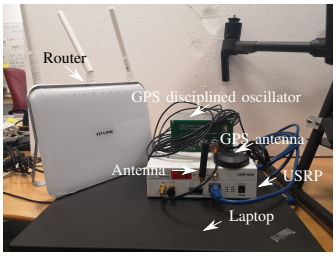

(c)

Fig. 1: The UAV measurement system. (a) The block diagram of the system. (b) Air part. (c) Ground part.

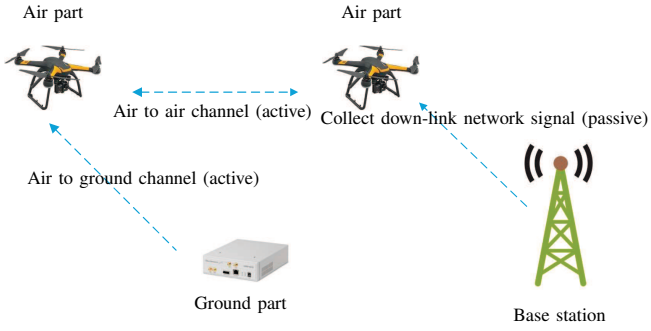

Fig. 2: The sketch of the UAV measurement system applied in the active (A2A and A2G channel) and passive (collect down-link signals from BS) measurement campaigns.

routers to control the air part from the ground. The USRPs can be programmed by GnuRadio or LabVIEW softwares in the computers to transmit and receive real-time signals at specific carrier frequency and with specific sampling rate (or bandwidth). The received data is also stored in the computer. Furthermore, transmitter and receiver parts are time-synchronized by the pulse per second (PPS) signals generated from the GPS modules and frequency-synchronized by the accurate 10 MHz reference signals provided by the GPS-disciplined clocks. As an example, a pseudo-noise (PN) sequence signal with a bandwidth of 20 MHz is transmitted repeatedly at the center frequency of 2.585 GHz and recorded with complex sampling rate of 25 MHz at the receiver. The channel impulse response (CIR) is calculated by the correlation between the transmitted and received signals.

III. System Response

To investigate the possible effect caused by the USRP devices and cables, a measurement was conducted by connecting two USRP devices with a cable used in the measurement campaigns directly. The baseband equivalent signal $s(t)$ with a bandwidth of 20 MHz was transmitted from the transmitter USRP device and received by the receiver USRP device as baseband equivalent signal $r(t)$.

Fig. 3(a) illustrates the normalized power frequency spectra of the transmitted signal $s(t)$ and received signal $r(t)$. Furthermore, the normalized power frequency spectra with the range of 150 KHz are plotted in Fig. 3(b). It can be observed that the spectrum of the received signal $r(t)$ is deteriorated near 0 Hz, which is probably due to direct-current (DC) leakage of the USRP. This effect can be ignored in the case of orthogonal frequency division multiplexing (OFDM) systems, since zero frequency point is not used.

Fig. 3(c) illustrates the normalized ideal instantaneous power delay profile (PDP) $|h_i(\tau)|^2$ and measured PDP $|h_m(\tau)|^2$, where

$$h_i(\tau) = \frac{\int s(t)s^*(t-\tau)dt}{\int s(t)s^*(t)dt}, \tag{1}$$

$$h_m(\tau) = \frac{\int r(t)s^*(t-\tau)dt}{\int s(t)s^*(t)dt}. \tag{2}$$

Note that the illustrated PDPs are over-sampled with sample interval as [1/(5×25e6)]. It can be observed that the effect of the equipment and cable can be ignored, when we consider the CIR within the dynamic range of 30 dB.

IV. Calibrate the Effects of Local Oscillator

The sampling rate and center frequency are determined based on the 10 MHz reference frequency provided by the local oscillator.[1] However, the inaccuracy of local oscillator can lead to the shifts of the sampling rate and center frequency from the expected or set values. Thus a GPS disciplined oscillator is usually used to increase the accuracy. Even so, the deviation is inevitable although smaller. Moreover, it cannot be guaranteed that GPS-disciplined clock is always available to increase the accuracy.

Figs. 4(a) and 4(b) illustrate the measured concatenated power delay profiles (CPDPs) and Doppler delay power spectra obtained in static state, respectively. It can be expected that the delay should be fixed and Doppler shift should be zero, since the transmitter and receiver are in static state. However, it can be observed from Fig. 4(a) that the delay is shifting and from Fig. 4(b) that a Doppler shift exists, due to the deviation of the sampling rate and center frequency caused by the inaccuracy of local oscillator. To solve the problem, we propose a post-processing method to calibrate sampling rate and center frequency as follows.

[1]The deviation of the reference frequency is time-variant and dependent on temperature, etc. The deviation tends to be stable after a specific time period (about half an hour) of warming up.

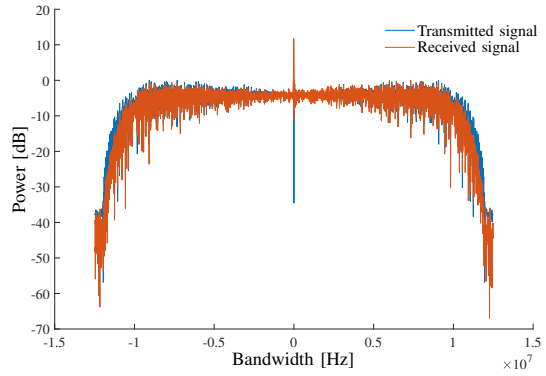

(a)

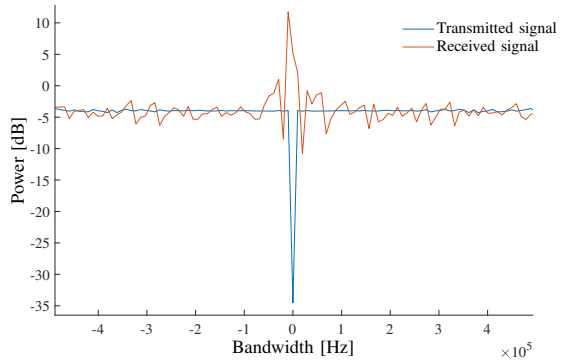

(b)

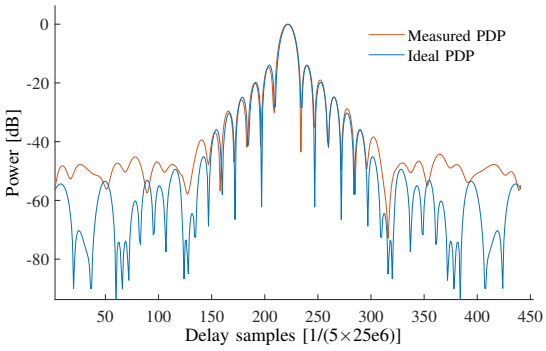

(c)

Fig. 3: The effects introduced by the system responses. (a) Power frequency spectra of transmitted signal and received signal. (b) Power frequency spectra with the range of 150 KHz. (c) Normalized ideal and measured PDPs.

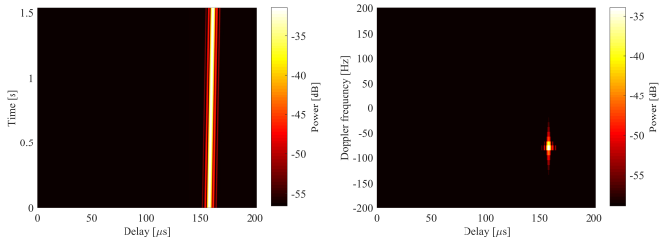

(a) (b)

Fig. 4: The measured CPDPs and Doppler delay power spectra obtained in static state. (a) CPDP. (b) Doppler delay power spectra.

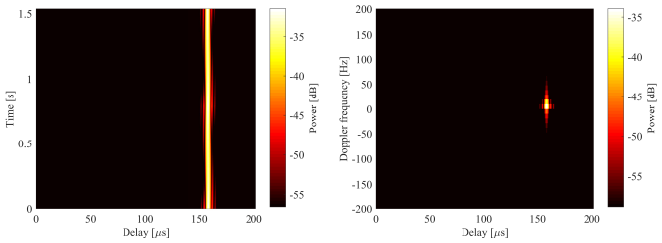

(a) (b)

Fig. 5: Calibrated CPDPs and Doppler delay power spectra obtained in static state. (a) CPDP. (b) Doppler delay power spectra.

Let us consider the reference frequencies provided by the local oscillators in both USRPs are f_{tx} and f_{rx}, respectively. Both f_{tx} and f_{rx} should be 10 MHz if no deviation exists. We denote the clock times at the transmit USRP and the receiver USRP as t and t', respectively. Then it can be known that

$$t = \frac{f_{\text{rx}}}{f_{\text{tx}}} t' + \tau_{\text{offset}} \tag{3}$$

or

$$t' = \frac{f_{\text{tx}}}{f_{\text{rx}}} t + \tau'_{\text{offset}} \tag{4}$$

where τ_{offset} is a fixed offset caused by the time-synchronization offset, i.e., the zero time at both USRPs may be different. When (3) is written as (4), τ_{offset} becomes τ'_{offset} which is still a fixed offset. The passband signal $s_p(t)$ transmitted can be formatted as

$$s_p(t) = \mathcal{R}\{s(t) \exp\{j2\pi f_c t\}\} \tag{5}$$

where f_c is the center frequency. As the two USRPs are connected using a cable, the received passband signal at the receiver USRP can be written as

$$r_p(t) = \mathcal{R}\{\alpha_0 s(t-\tau_0) \exp\{j2\pi f_c (t-\tau_0)\} \tag{6}$$

where α_0 and τ_0 denote the complex attenuation and delay, respectively. When the passband signal $r_p(t)$ is demodulated at the receiver to obtain its baseband equivalent signal, $\exp\{-j2\pi f_c t'\}$ is applied to move its spectrum down. Therefore, it can be known that

$$r(t) = \alpha_0 s(t-\tau_0) \exp\{j2\pi f_c (t-t') - j2\pi f_c \tau_0\} \tag{7}$$

Replace t with the clock time t' at the receiver according to (3) or (4), we have

$$r(t') = \alpha_0 s(\frac{f_{\text{rx}}}{f_{\text{tx}}} t' + \tau_{\text{fixed}}) \exp\{j2\pi f_c (\frac{f_{\text{rx}}}{f_{\text{tx}}} - 1) t' + j2\pi f_c \tau_{\text{fixed}}\} \tag{8}$$

with

$$\tau_{\text{fixed}} = \tau_{\text{offset}} - \tau_0 \tag{9}$$

It is straightforward to know the fact from (8) that the baseband signal received at the receiver has a "fake" Doppler frequency as $f_c(\frac{f_{\text{rx}}}{f_{\text{tx}}} - 1)$ as illustrated in Fig. 4(b). Moreover, if the transmitted signal has a period of T, the received period will become $T\frac{f_{\text{tx}}}{f_{\text{rx}}}$ which is the reason for the shifting delay in the CPDPs as illustrated in Fig. 4(a). Figs. 5(a) and

5(b) illustrate the calibrated CPDPs and Doppler delay power spectra, respectively. It can be observed that the delay shift with respect to time and Doppler frequency are calibrated to zero, which indicates the validity of the post-processing method.

V. Conclusion

In this contribution, a USRP-based channel sounding system for characterizing the unmanned-aerial-vehicle (UAV) channel is introduced. It is found that the effect of the equipment and cable can be ignored. Besides, a post-processing method is proposed to eliminate the effects of local oscillator in the actual measurement activities. The method requires a static pre-measurement and is necessary especially when the Global Positioning System (GPS) disciplined oscillator is unavailable such as in mountain areas, high-speed railway and tunnels in subway scenarios. The future research mainly focuses on the following aspects: *i)* The system will be further applied for the virtual linear or circular array measurements, based on the up to centimetre-level real-time kinematic (RTK) positioning function. *ii)* The system can be used for air-to-air (A2A) channel measurement, which has not been widely investigated. *iii)* The system will be applied to evaluate the 4G and 5G communication techniques, e.g. the performance of different waveforms [15].

References

[1] Y. Zeng, R. Zhang, and T. J. Lim, "Wireless communications with unmanned aerial vehicles: opportunities and challenges," *IEEE Communications Magazine*, vol. 54, no. 5, pp. 36–42, 2016.

[2] X. Cai, J. Rodriguez-Pineiro, X. Yin, N. Wang, B. Ai, G. F. Pedersen, and A. P. Yuste, "An empirical air-to-ground channel model based on passive measurements in LTE," *IEEE Transactions on Vehicular Technology*, vol. 68, no. 2, pp. 1140–1154, 2019.

[3] A. A. Khuwaja, Y. Chen, N. Zhao, M. S. Alouini, and P. Dobbins, "A survey of channel modeling for UAV communications," *IEEE Communications Surveys and Tutorials*, vol. 20, no. 4, pp. 2804–2821, 2018.

[4] X. Ye, X. Cai, X. Yin, J. Rodriguez-Pineiro, L. Tian, and J. Dou, "Air-to-ground big-data-assisted channel modeling based on passive sounding in LTE networks," *IEEE Globecom Workshops, GC Workshops Proceedings*, pp. 1–6, 2018.

[5] R. M. Gutierrez, H. Yu, Y. Rong, and D. W. Bliss, "Time and frequency dispersion characteristics of the UAS wireless channel in residential and mountainous desert terrains," *14th IEEE Annual Consumer Communications and Networking Conference*, pp. 516–521, 2017.

[6] B. Van Der Bergh, A. Chiumento, and S. Pollin, "LTE in the sky: Trading off propagation benefits with interference costs for aerial nodes," *IEEE Communications Magazine*, vol. 54, no. 5, pp. 44–50, 2016.

[7] W. Khawaja, O. Ozdemir, and I. Guvenc, "UAV air-to-ground channel characterization for mm-Wave systems," *IEEE Vehicular Technology Conference*, pp. 1–5, 2018.

[8] A. Al-Hourani and K. Gomez, "Modeling cellular-to-UAV path-loss for suburban environments," *IEEE Wireless Communications Letters*, vol. 7, no. 1, pp. 82–85, 2 2018.

[9] W. Khawaja, I. Guvenc, and D. Matolak, "UWB channel sounding and modeling for UAV air-to-ground propagation channels," *IEEE Global Communications Conference (GLOBECOM)*, pp. 1–7, 2016.

[10] R. Amorim, H. Nguyen, P. Mogensen, I. Z. Kovács, J. Wigard, and T. B. Sørensen, "Radio channel modeling for UAV communication over cellular networks," *IEEE Wireless Communications Letters*, vol. 6, no. 4, pp. 514–517, Aug 2017.

[11] A. Al-Hourani and K. Gomez, "Modeling cellular-to-UAV path-loss for suburban environments," *IEEE Wireless Communications Letters*, vol. 7, no. 1, pp. 82–85, Feb 2018.

[12] L. Afonso, N. Souto, P. Sebastiao, M. Ribeiro, T. Tavares, and R. Marinheiro, "Cellular for the skies: Exploiting mobile network infrastructure for low altitude air-to-ground communications," *IEEE Aerospace and Electronic Systems Magazine*, vol. 31, no. 8, pp. 4–11, Aug 2016.

[13] E. Vitucci, M. Arpaio, M. Barbiroli, V. Semkin, V. Degli-Esposti, and F. Fuschini, "Air-to-ground propagation channel characterization. ray-launching simulations and channel measurements." in *EURO-COST Conference*, May 2019.

[14] X. Cai, A. Gonzalez-Plaza, D. Alonso, L. Zhang, C. B. Rodriguez, A. P. Yuste, and X. Yin, "Low altitude UAV propagation channel modelling," *11th European Conference on Antennas and Propagation*, pp. 1443–1447, 2017.

[15] T. Dominguez-Bolano, J. Rodriguez-Pineiro, J. A. Garcia-Naya, and L. Castedo, "The GTEC 5G link-level simulator," *1st International Workshop on Link and System Level Simulations (IWSLS)*, pp. 1–6, 2016.